Endothelin-1–Induced Spreading Depression in Rats Is Associated with a Microarea of Selective Neuronal Necrosis

Jens P. Dreier,*,†,[1] Jörg Kleeberg,‡ Mesbah Alam,* Sebastian Major,*,† Matthias Kohl-Bareis,§ Gabor C. Petzold,|| Ilya Victorov,¶ Ulrich Dirnagl,*,† Tiho P. Obrenovitch,# and Josef Priller*,**

*Department of Experimental Neurology and †Department of Neurology, Charité Universitätsmedizin, Berlin, Berlin, Germany, ‡Department of Neurology, Centre Universitaire Hospitalier Vaudois, Lausanne, Switzerland; §RheinAhrCampus Remagen, University of Applied Sciences Koblenz, Remagen, Germany; ||Department of Molecular and Cellular Biology, Harvard University, Cambridge, Massachusetts; ¶Laboratory of Experimental Neurocytology, Brain Research Institute, Moscow, Russia; #Pharmacology, School of Pharmacy, University of Bradford, Bradford, UK; and **Laboratory of Molecular Psychiatry, Department of Psychiatry and Psychotherapy, Charité Universitätsmedizin Berlin, Germany

Two different theories of migraine aura exist: In the vascular theory of Wolff, intracerebral vasoconstriction causes migraine aura *via* energy deficiency, whereas in the neuronal theory of Leão and Morison, spreading depression (SD) initiates the aura. Recently, it has been shown that the cerebrovascular constrictor endothelin-1 (ET-1) elicits SD when applied to the cortical surface, a finding that could provide a bridge between the vascular and the neuronal theories of migraine aura. Several arguments support the notion that ET-1–induced SD results from local vasoconstriction, but definite proof is missing. If ET-1 induces SD *via* vasoconstriction/ischemia, then neuronal damage is likely to occur, contrasting with the fact that SD in the otherwise normal cortex is not associated with any lesion. To test this hypothesis, we have performed a comprehensive histologic study of the effects of ET-1 when applied topically to the cerebral cortex of halothane-anesthetized rats. Our assessment included histologic stainings and immunohistochemistry for glial fibrillary acidic protein, heat shock protein 70, and transferase dUTP nick-end labeling assay. During ET-1 application, we recorded (i) subarachnoid direct current (DC) electroencephalogram, (ii) local cerebral blood flow by laser-Doppler flowmetry, and (iii) changes of oxyhemoglobin and deoxyhemoglobin by spectroscopy. At an ET-1 concentration of 1 μM, at which only 6 of 12 animals generated SD, a microarea with selective neuronal death was found only in those animals demonstrating SD. In another five selected animals, which had not shown SD in response to ET-1, SD was triggered at a second cranial window by KCl and propagated from there to the window exposed to ET-1. This treatment also resulted in a microarea of neuronal damage. In contrast, SD invading from outside did not induce neuronal damage in the absence of ET-1 ($n = 4$) or in the presence of ET-1 if ET-1 was coapplied with BQ-123, an ET_A receptor antagonist ($n = 4$). In conclusion, SD in presence of ET-1 induced a microarea of selective neuronal necrosis no matter where the SD originated. This effect of ET-1 appears to be mediated by the ET_A receptor. Exp Biol Med 232:204–213, 2007

Key words: migraine aura; spreading depression; endothelin-1; stroke; vasospasm

Introduction

Migraine aura is the transient neurologic deficit that precedes migraine headache in 10% to 30% of migraineurs. It can affect different modalities such as vision, language, and sensory and motor function. The characteristic of the aura is the slow spread of the neurologic symptoms. The most common aura involves the vision, with hallucinations of bright flashing lights and partial blindness that slowly spread in one visual hemi-field.

There are two different pathophysiological theories of the aura. In the 1930s, Wolff coined the vascular theory, in which intracerebral vasoconstriction is the primary event, leading to a secondary neuronal disturbance through energy deficiency (1). Thus, according to Wolff, the aura was the

This study was supported by grant DFG DR 323/2–2 (J.P.D.) and DFG SFB 507 A5 (J.P.). Support of the Hermann and Lilly Schilling foundation (U.D.) is gratefully acknowledged.

[1] To whom correspondence should be addressed at Department of Neurology, Charité, Humboldt Universität, Schumannstr. 20/21, 10117 Berlin, Germany. E-mail: jens.dreier@charite.de

Received October 20, 2005.
Accepted July 7, 2006.

1535-3702/07/2322-0204$15.00

psychologic correlate of a neuronal disturbance that occurs secondary to ischemia. He did not characterize the kind of neuronal disturbance any further. In seeming contrast, in 1945 Leão and Morison proposed the neuronal theory, in which spreading depression (SD) is the pathophysiological correlate of the aura (2). SD is a depolarization wave of neurons and astrocytes that propagates across the cerebral cortex at a rate of approximately 3 mm/min. During SD, energy demand increases, triggering a transient increase of local cerebral blood flow (CBF) that is followed by long-lasting oligemia. No neuronal damage is induced by SD under normal conditions, which corresponds with the fact that migraine aura is not usually associated with any brain damage (3).

The SD theory of the migraine aura by Leão and Morison (2) was based on the observation that SD in the rabbit cortex propagated in a similar fashion to the visual and sensory hallucinations of patients with migraine aura. Leão and Morison did not induce SD *via* artificial vasoconstriction but by a direct current stimulus to the rabbit cortex. Based on this finding and the presumed relation between SD and migraine aura, they proposed that the migraine aura is not induced by vasoconstriction but is caused by a primary disturbance of the neuronal network.

It is now increasingly recognized that SD is indeed the pathophysiological correlate of the migraine aura, based on clinical studies with single–photon-emission computed tomography, positron emission tomography, or functional magnetic resonance imaging (4, 5). However, at least in some patients, there is clinical evidence supporting Wolff's notion that migraine aura can be caused by a primarily vascular disturbance: (i) Migraine aura can be triggered by cerebral angiography (6, 7) or in the presence of a vascular disease such as carotid artery dissection, fibromuscular dysplasia (8), or genetically transmitted microangiopathies like cerebral autosomal dominant arteriopathy with subcortical infarcts and leukencephalopathy (9). (ii) There are angiographic and Doppler-sonographic observations of short-term vasospasm in large cervicocephalic vessels related to migraine attacks (10). (iii) Furthermore, all recent population- and hospital-based studies showed a significantly increased risk for migraineurs with aura to suffer from ischemic stroke (11).

Recently, it has been discovered that endothelin-1 (ET-1), a very potent cerebrovascular constrictor (12), is also a very potent *in vivo* inducer of SD (13). This finding may provide a bridge between Wolff's vascular and Leão and Morison's neuronal theory of the migraine aura if Wolff's vascular theory is reformulated in the following way: Intracerebral vasoconstriction is the cause of migraine aura in a fraction of patients in whom vasoconstriction produces a microarea of ischemia, which in turn gives rise to SD. SD, from there, invades normal tissue, where it produces the visual or sensory hallucinations referred to as migraine aura.

Several reports have previously implicated the involvement of ET-1 in the pathogenesis of migraine, based on increased plasma levels of ET-1 during migraine attacks (14–16). A link between migraine and endothelins has also been suggested in a population-based study demonstrating an association between migraine and an endothelin type A receptor gene polymorphism (17).

However, the peptide ET-1 is not only a vasoconstrictor, but also a neuronal and astroglial modulator, and to date it has remained unclear which direct cellular target of ET-1 mediates SD initiation (18). If cerebrovascular smooth muscle is the target, with vasoconstriction triggering SD *via* energy deficiency, then neuronal damage would be expected. Therefore, we carried out a comprehensive histologic study of cortical tissue subjected to ET-1–induced SD. This was supplemented by an investigation of ET-1–induced changes of the subarachnoid direct current (DC) potential with an Ag-AgCl electrode to detect SD of CBF using laser-Doppler flowmetry, and changes in oxyhemoglobin (Δoxy-Hb) and deoxyhemoglobin (Δdeoxy-Hb) concentrations by spectroscopy.

Materials and Methods

Animals. All animal experiments conformed to institutional guidelines and were approved by an official committee. Male Wistar rats ($n = 28$; 280–420 g) used for the histologic study were anesthetized with halothane (1.5% in 30% O_2 and 70% N_2O). In these animals the tail artery was cannulated to measure blood pressure and arterial blood gases. The other rats ($n = 11$; 280–420 g) were anesthetized with 100 mg/kg thiopental-sodium intraperitoneally (ip; Trapanal, BYK Pharmaceuticals, Konstanz, Germany), tracheotomized, and artificially ventilated (Effenberger Rodent Respirator; Effenberger Med.-Techn. Gerätebau, Pfaffing/Attel, Germany). The left femoral artery and vein were cannulated, and a saline solution was continuously infused at 1 ml/hr. Body temperature was maintained at 38.0 ± 0.5°C using a heating pad. Systemic arterial pressure (RFT Biomonitor, Zwönitz, Germany) and end-expiratory pCO_2 (CO_2 Monitor EGM I; Heyer, Bad Ems, Germany) were monitored. PaO_2, $PaCO_2$, and pH were serially measured using a Compact 1 Blood Gas Analyser (AVL Medizintechnik GmbH, Bad Homburg, Germany). Because the rats were not paralyzed, the adequacy of the level of anesthesia was assessed by testing motor responses to tail pinching. In addition, changes of blood pressure in response to tail pinching were used to control anesthesia. Further thiopental doses (25 mg/kg ip) were applied when necessary.

A craniotomy was performed over the somatosensory cortex using a saline-cooled drill and a cranial window was implanted as previously described (13). The dura mater was removed. In animals, in which spectroscopy at visible wavelengths was applied, the craniotomy site was covered with a piece of glass cut from a coverslip. Inflow and outflow tubes allowed us to superfuse the brain cortex with artificial cerebrospinal fluid (ACSF) at the closed window.

Only the inflow tube was necessary for open windows. The composition of the ACSF in m*M* was: Na^+, 152; K^+, 3; Ca^{2+}, 1.5; Mg^{2+}, 1.2; HCO_3^-, 24.5; Cl^-, 135; glucose, 3.7; urea, 6.7. The ACSF was equilibrated with a gas mixture containing 6.6% O_2, 5.9% CO_2, and 87.5% N_2. A pO_2 between 90 and 130 mm Hg, a pCO_2 between 35 and 45 mm Hg, and a pH between 7.35 and 7.45 were accepted as physiological. Local CBF was continuously monitored by two laser-Doppler flow probes (Perimed AB, Järfälla, Sweden). Different fiber separations in the laser probes allowed us to measure CBF at different cortical depths in Group 1. The caudal laser probe recorded both the CBF changes at a depth of around 0.5 mm (fiber separation: 140 μm) and between 1 and 1.5 mm (fiber separation: 500 μm), and the rostral laser probe at a depth between 0.5 and 1 mm (fiber separation: 250 μm). The DC electroencephalogram (DC-EEG) was measured with an Ag-AgCl electrode placed in the subarachnoid space. The electrode was connected to a differential amplifier (Jens Meyer, Munich, Germany). CBF and DC potential were continuously recorded using a personal computer and a chart recorder (DASH IV; Astro-Med, Inc., West Warwick, RI). Alternating current EEG was continuously recorded with the chart recorder.

Animals, if not assigned to histologic analysis, were immediately killed after the experiment by intravenous administration of concentrated KCl solution. In case of later histologic analysis, the wounds were treated with lidocaine-hydrochloride gel (2%; Astra GmBH, Wedel, Germany) and sutured. The opioid buprenorphine (0.5 mg/kg body wt sc; Boehringer, Mannheim, Germany) was administered as postoperative analgesic and rats were allowed to recover from anesthesia. Twenty-four hours after the experiment, cardiac perfusion fixation was performed under deep anesthesia with thiopental sodium.

Cortical Δoxy-Hb and Δdeoxy-Hb Concentration Changes Measured by Spectroscopy at Visible Wavelengths. Changes in light attenuation ($\lambda = 500$–800 nm) were measured with a custom-built system consisting of a halogen light source (LOT Oriel, Darmstadt, Germany) and a spectrometer (S2000, Ocean Optics, Dunedin, FL). Changes in the tissue chromophore concentrations of oxy-Hb and deoxy-Hb (Δc_i) were calculated based on a modified Lambert-Beer law

$$\Delta A(\lambda) = \sum [\varepsilon_i(\lambda) \cdot \Delta c_i \cdot D_a(\lambda)],$$

where ΔA is the change in attenuation, and ε_i are the extinction coefficients of the chromophores. D_a is a correction term for the path length. D_a is wavelength-dependent, as it depends on the absorption and scattering properties of the tissue. D_a can be estimated from Monte Carlo simulations of the photon propagation in tissue. The description of the experimental data is significantly improved when this correction term is used. Details of the analysis are given by Kohl et al. (19).

Histology and Immunocytochemistry. *Histochemistry.* Twenty-four hours after the experiment, animals were perfused transcardially with modified Lillie fixative as previously described (20). The brains were embedded in paraffin wax, and 8–10 μm frontal or parasagittal sections were stained with cresyl violet, hematoxylin-eosin, and vanadium acid fuchsin–toluidine blue (VAF). Frontal sectioning started at a distance of 2 mm from the window area; parasagittal sections were cut equidistantly throughout both hemispheres. Adjacent sections were obtained every 200 μm.

Immunohistochemistry and Transferase dUTP Nick-End Labeling (TUNEL) Assay. Based on the histochemical data, 5–12 representative sections per brain were chosen for immunohistochemistry and TUNEL assay. The sections were deparaffinized, quenched for endogenous peroxidase activity, and incubated overnight with the primary antibodies: rabbit polyclonal antiglial fibrillary acidic protein (GFAP; Dako, Carpinteria, CA) and mouse monoclonal anti–heat shock protein 70 (HSP70; Stressgen, Victoria, Canada) at dilutions of 1:5000 and 1:200, respectively. Secondary biotinylated goat–anti-rabbit or horse–anti-mouse antibodies (Vector, Burlingame, CA) were applied at a dilution of 1:100 for 90 mins at room temperature. Visualization was achieved using the Vectorstain ABC elite kit (Vector) reacted with 3,3′-diaminobenzidine/H_2O_2 (Sigma Chemicals, Deisenhofen, Germany). Omission of primary antibodies served as negative control. The TUNEL assay was performed using the Apoptag Kit (Intergen, Oxford, UK) according to the manufacturer's protocol. Omission of terminal deoxynucleotidyl transferase reaction served as negative control.

Experimental Protocols. *Group 1.* To begin with, neuropathologic changes were studied in 15 animals, 6 of which had developed SD in response to ET-1 (Sigma Chemicals) at 1 μ*M*, and 6 of which did not respond with SD within 1 hr of equilibration with ET-1. In order to detect ET-1–induced SD, CBF and DC changes were recorded. Three sham control animals with cranial windows did not receive ET-1. Furthermore, one rat without craniotomy was investigated for comparison.

Group 2. In this series, two cranial windows were implanted over the same hemisphere. Window 1 was initially superfused with physiological ACSF, whereas Window 2 was superfused with ACSF containing 1 μ*M* ET-1. If the animal did not develop SD in response to ET-1 within 1 hr of equilibration, the K^+ concentration in the ACSF ($[K^+]_{ACSF}$) at Window 1 was increased to 130 m*M* in order to induce SD at Window 1 (the Na^+ concentration in the ACSF of Window 1 was lowered accordingly to maintain iso-osmolarity; $n = 5$). Then, SD propagated from Window 1 to Window 2, which was continuously superfused with ET-1. The propagation of SD from Window 1 to Window 2 was verified using a subarachnoid Ag-AgCl electrode and a laser-Doppler probe (fiber separation 250 μm) in each window. After the first SD, the ACSF containing elevated $[K^+]_{ACSF}$ (Window 1) and the ACSF

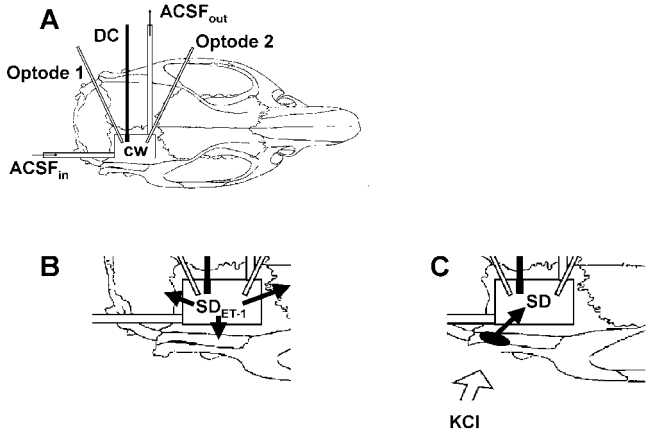

Figure 1. (A) Experimental setup for Groups 5 and 6. The closed window was covered with a piece of glass cut from a coverslip. An inflow ($ACSF_{in}$) and outflow ($ACSF_{out}$) tube allowed the superfusion of the cortex with either physiological ACSF (Group 6) or ACSF containing ET-1 (Group 5). The changes of the cortical oxy-Hb and deoxy-Hb concentrations were measured with optodes at the rostral and caudal thirds of the window (Optode 1 and 2). The DC shift was recorded using an Ag-AgCl electrode. (B) Larger magnification of (A) demonstrating an ET-1–induced SD (SD_{ET-1}) that spread from the window area to other cortical fields (Group 5). (C) Experimental setup of the control animals in Group 6. SD was remotely induced at an open window using a drop of KCl (300 m*M*). From the open window, SD spread to the closed window where the cortex was superfused with physiological ACSF, and the changes of oxy-Hb and deoxy-Hb as well as the DC potential were measured.

containing ET-1 (Window 2) were immediately washed out. As in Group 1, the neuropathologic outcome was determined. The purpose of this group was to investigate whether SD, if invading from outside, would cause neuronal damage in a cortical area exposed to ET-1.

Group 3. This group served as a control for Group 2. SD was similarly induced by high $[K^+]_{ACSF}$ at Window 1, but physiological ACSF was applied at Window 2 instead of ACSF containing ET-1.

Group 4. In Group 4, we determined whether the SD-induced neuronal damage in presence of ET-1 was related to an endothelin A (ET_A) receptor activation. For this purpose, similarly to the procedure for Groups 2 and 3, SD was induced by high $[K^+]_{ACSF}$ at Window 1 but ET-1 (1 μ*M*) was coapplied with the ET_A receptor antagonist BQ-123 at Window 2 (5 μ*M*; Sigma Chemicals).

Groups 5 and 6. Differences between SDs in presence of ET-1 (Group 5, $n = 6$) and remotely induced SDs in presence of physiological ACSF (Group 6, $n = 5$) were studied regarding cortical Δoxy-Hb and Δdeoxy-Hb. The experimental setup is shown in Figure 1.

Data Analysis. Data were analyzed by comparing relative changes of CBF and absolute changes of the DC potential, oxy-Hb, and deoxy-Hb. CBF changes were calculated in relation to baseline at the onset of the experiment (=100%). All data in text and figures are given as mean value ± standard deviation. Statistical comparisons were performed using either a two-sample or a paired *t* test. $P < 0.05$ was accepted as statistically significant.

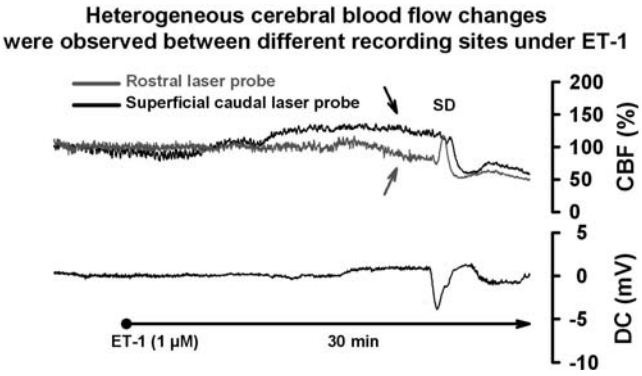

Figure 2. Representative ET-1–induced SD, showed by a negative shift of the DC potential, with associated changes in CBF. Two laser-Doppler flow probes were positioned over the cortex at the caudal and rostral third of the cranial window. Different fiber separations in the laser probes allowed to measure local CBF in different cortical depths. As the CBF traces show, CBF was rather heterogeneous between the two recording sites (arrows). There was a marked decrease in CBF at the rostral laser probe before the first SD and a simultaneous marked increase at the caudal laser probe. The hemodynamic response to SD consisted of a small initial decrease followed by a spreading hyperemia and a pronounced spreading oligemia.

Results

The systemic variables remained within physiological limits throughout the experiments.

ET-1–Induced SDs Are Associated with a Microarea Exhibiting Selective Neuronal Death at the Superfusion Site (Group 1). Of 12 animals receiving ET-1 (1 μ*M*) under halothane anesthesia, only 6 developed SD, whereas 100% of animals under thiopental anaesthesia showed ET-induced SD in a previous study (13, 18). Before SD, CBF slightly increased to 112% ± 37% at the rostral laser probe ($probe_1$), to 114% ± 17% at the deep caudal laser probe ($probe_2$) and to 106% ± 23% at the superficial caudal laser probe ($probe_3$). The local CBF responses were often rather heterogeneous between rostral and caudal recording sites within individual experiments, with a pronounced decrease at one probe and a simultaneous pronounced increase at the other (Fig. 2). SD was characterized by a negative DC shift of –3.5 ± 0.9 mV lasting for 129 ± 8 secs. The hemodynamic response to SD consisted of a small initial decrease followed by a spreading hyperemia ($probe_1$, 146% ± 62%; $probe_2$, 131% ± 7%; $probe_3$, 125% ± 17%) and a spreading oligemia ($probe_1$, 71% ± 32%; $probe_2$, 68% ± 11%; $probe_3$, 62% ± 8%). There was a delay of 20 ± 11 secs between the two recording sites, consistent with propagation of the CBF changes. Interestingly, the average effect of ET-1 on resting CBF was not different between animals that eventually showed SD and those that did not. There was also no difference between resting CBF in animals receiving ET-1 and controls. However, in contrast to the individual recordings under ET-1, CBF was more stable and homogeneous between rostral and caudal recording sites in controls.

All those animals in which ET-1 induced SDs (between

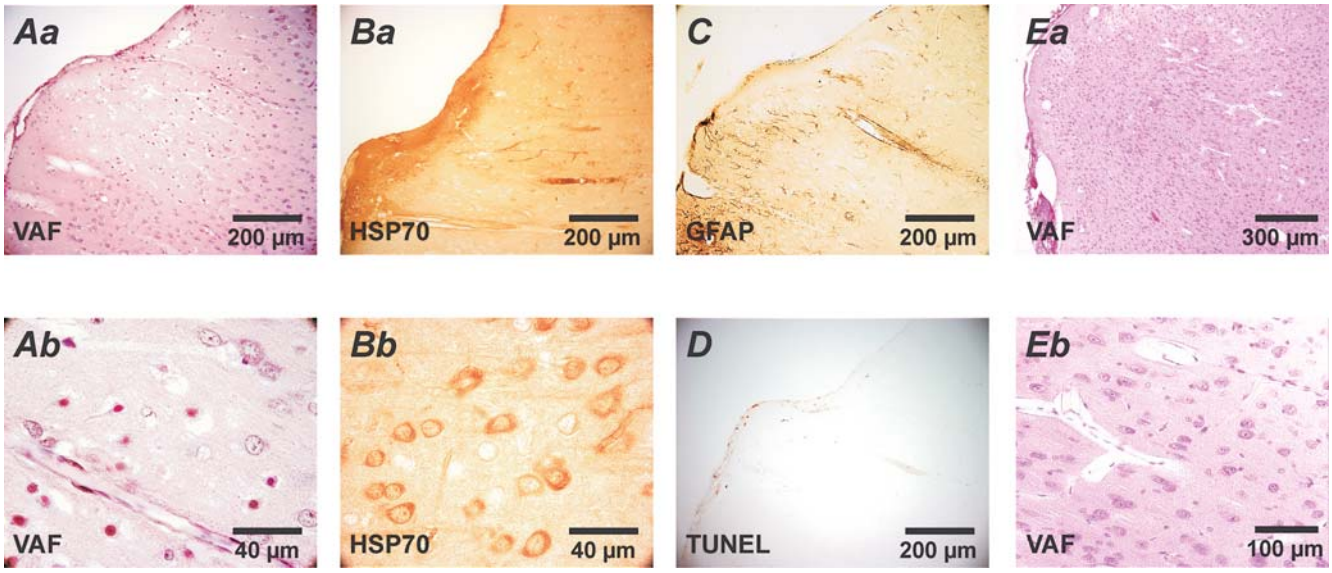

Figure 3. Histologic changes at the site of ET-1 application to the cortical surface, 24 hrs post-treatment. (Aa) Only those animals in which ET-1 induced SD demonstrated a microarea with selective neuronal death at the window site. The microarea of neuronal damage is completely surrounded by normal tissue. The section with the largest extent of the lesion is shown. Staining was performed with VAF. (Ab) Larger magnification of (Aa). Shrunken, hyperchromatic, acidophilic neurons with perineuronal halo are observed, indicating necrosis 24 hrs after ET-1–induced SD. Some surviving neurons, identified by the prominent nucleolus, are seen in the neighborhood. (Ba, Bb) Neurons surrounding the area of damage were morphologically intact, but generally showed strong HSP70 immunoreactivity. (C) GFAP immunoreactivity did not reveal obvious differences in the distribution of positive astrocytes between the area of neuronal damage and other cortical regions. Compared with a naïve brain, a slight to moderate increase of GFAP expression was found throughout the brain after craniotomy. (D) TUNEL was negative, suggesting that apoptosis was not the primary mechanism of cellular damage. (Ea) Animals in which ET-1 did not induce SD showed no microarea of necrosis. Staining was performed with VAF. (Eb) shows a larger magnification of (Ea).

1 and 3) were killed after 24 hrs. Sections stained with VAF showed hyperchromatic, acidophilic neurons with perineuronal halo (Fig. 3Aa and Ab). None of these cells were TUNEL-positive (Fig. 3D). The damaged neurons were few in number and confined to a small area close to the cortical surface where ET-1 had been superfused (Fig. 3Aa and Ab). Surrounding neurons were morphologically intact, but generally showed strong HSP70 immunoreactivity (Figs. 3Ba and Bb). The distribution of GFAP-positive astrocytes was not significantly different in the region of neuronal damage compared with other cortical regions (Fig. 3C). As previously described, GFAP immunoreactivity was slightly to moderately increased throughout the brain 24 hrs after craniotomy (20). No interhemispheric differences in GFAP expression were detectable at 24 hrs, which is consistent with data published by Herrera et al. (21) who showed that an ipsilateral rise of GFAP immunoreactivity occurred only between Days 2 and 7 after SD. No TUNEL-positive neurons were detected, suggesting that apoptosis was not the primary mechanism of cellular damage.

ET-1 did not induce neuronal necrosis in animals that had not generated SD as revealed by VAF staining (Fig. 3Ea and Eb). HSP70 immunoreactivity in the window area was also less pronounced in these animals. Similar data were obtained with VAF, GFAP, HSP70, and TUNEL stainings in 3 animals treated with physiological ACSF instead of ET-1 (control) and in those animals in which ET-1 did not elicit SD. In one animal superfused with ET-1, the window area was damaged during histologic processing. In another rat, subarachnoid hemorrhage was accidentally induced. In the latter case, widespread neuronal cell death, TUNEL staining, and pronounced expression of HSP70 and GFAP were detected in the cortex of both hemispheres (data not shown).

In summary, ET-1 produced a microarea of selective neuronal damage only in animals that displayed SD.

SD Invasion of the Cortical Window Under Study from Outside Induced a Microarea with Selective Neuronal Death in Cortex Exposed to ET-1 (Group 2). Artificial increase of $[K^+]_{ACSF}$ to 130 m*M* in Window 1 induced SD in all experiments. The SD-related parameters did not show a significant difference between Window 1 ($[K^+]_{ACSF}$, 130 m*M*) and Window 2 (ET-1, 1 µ*M*) apart from the subarachnoid negative DC shift, which was significantly larger in presence of high $[K^+]_{ACSF}$ (Table 1). This difference was consistent with previous findings that SD is associated with a larger subarachnoid negative DC shift in presence of high $[K^+]_{ACSF}$ (22).

In all the animals of this group ($n = 5$), the histologic changes at Window 2 (ET-1) included a region with hyperchromatic, acidophilic neurons typical of necrosis. This pattern was similar to that observed in animals of Group 1, in which ET-1 directly elicited SD. In contrast to Window 2, typical histologic changes associated with increased $[K^+]_{ACSF}$ were seen at Window 1. Neurons were

Table 1. SD-Related Parameters of the Two-Window Experiments[a]

Group	Window	Treatment	CBF_{pre} (%)	CBF_{hyper} (%)	CBF_{olig} (%)	DC potential (mV)	DC_{Dur} (secs)	Propagation time (secs)
2	1	$[K^+]_{ACSF}$ (130 m*M*)	105 ± 26	142 ± 39	111 ± 30	−5.8 ± 1.4	140 ± 44	69 ± 46
	2	ET-1 (1 μ*M*)	90 ± 14	133 ± 22	77 ± 32	−2.9 ± 0.5*	138 ± 38	
3	1	$[K^+]_{ACSF}$ (130 m*M*)	110 ± 28	130 ± 50	88 ± 53	−5.5 ± 2.2	137 ± 65	80 ± 36
	2	Physiological ACSF	95 ± 16	117 ± 26	63 ± 18	−3.2 ± 0.5	121 ± 44	
4	1	$[K^+]_{ACSF}$ (130 m*M*)	93 ± 16	114 ± 16	93 ± 18	−3.9 ± 1.5	142 ± 54	60 ± 64
	2	ET-1 (1 μ*M*) + BQ-123 (5 μ*M*)	96 ± 14	118 ± 12	68 ± 13	−2.9 ± 1.0	126 ± 47	

[a] CBF_{pre}, CBF value immediately before the first SD; CBF_{hyper}, CBF value during SD-induced hyperemia; CBF_{olig}, lowest CBF value after SD; DC_{Dur}, duration of the SD-associated negative DC shift; propagation time, delay between the DC responses in window 1 and 2.
* $P < 0.05$ (paired *t* test).

not acidophilic. They had a scalloped appearance with pronounced perineuronal and perivascular swelling.

SD Invasion of the Cortical Window Under Study from Outside Did Not Induce a Microarea with Selective Neuronal Death in Cortex Exposed to Physiological ACSF (Group 3). No statistically significant differences in the SD-related parameters were observed between windows 1 and 2 in this control group ($n = 4$, Table 1). The histologic changes at Window 1 ($[K^+]_{ACSF}$, 130 m*M*) were similar to those at Window 1 of Group 2 in that perineuronal and perivascular swelling was observed. VAF staining did not reveal hyperchromatic, acidophilic neurons at either Window 1 or Window 2. HSP70 immunoreactivity was almost undetectable. As in Groups 1 and 2, mild astrogliosis was observed.

SD Invasion of the Cortical Window Under Study from Outside Did Not Induce a Microarea with Selective Neuronal Death in Cortex Exposed to the Combination of ET-1 with the ET_A Receptor Antagonist BQ-123 (Group 4). Again, no statistically significant differences of the SD-related parameters were observed between Windows 1 and 2 in this group ($n = 4$, Table 1). The histologic changes at Window 1 ($[K^+]_{ACSF}$, 130 m*M*) were similar to those at Window 1 of Groups 2 and 3. Hematoxylin and eosin staining revealed edematous changes at Window 1 (Fig. 4Aa and Ab). No microareas of neuronal death were observed at either Window 1 or Window 2 using hematoxylin and eosin staining (Fig. 4Aa, Ab, Ba, and Bb) and VAF staining. As in Groups 1–3, GFAP immunoreactivity was mildly to moderately increased throughout the cortex (Fig. 4C–E). Some neurons surrounding both window areas demonstrated mild HSP70 immunoreactivity (Fig. 4F).

Changes in Oxy-Hb and Deoxy-Hb Concentration in Response to SD Are Qualitatively Similar in Presence or Absence of ET-1 (Groups 5, 6). In a model of middle cerebral artery occlusion, penumbral SDs were distinguished from normal SDs by an initial decrease of oxy-Hb and increase of deoxy-Hb (23). In order to test whether ET-1–induced SDs show similar abnormalities, a closed cranial window was implanted in 11 animals to compare the changes in cortical oxy-Hb and deoxy-Hb concentrations that were associated with SD when SD was elicited under ET-1 and under normal conditions (Fig. 1). Δoxy-Hb and Δdeoxy-Hb were measured relative to baseline at the rostral and caudal third of the window using spectroscopy at visible wavelengths (measuring depth approximately 200 μm). The subarachnoid DC potential and EEG were also recorded.

In five controls (i.e., cortical window perfused with physiological ACSF, and SD remotely induced by KCl), Δoxy-Hb and Δdeoxy-Hb values were similar to those previously measured during SD (Fig. 5A; see Ref. 24). In six other animals (cortex superfusion with 1 μ*M* ET-1), the signals were not qualitatively different, but the average of rostral and caudal oxy-Hb was mildly but significantly lower before, during, and after the first SD compared with the values recorded in the presence of physiological ACSF (Fig. 5A). Δdeoxy-Hb was significantly different only after the first SD in the presence of ET-1 (Fig. 5A). Figure 6 shows a recording of Δoxy-Hb and Δdeoxy-Hb during a cluster of ET-1–induced SDs. Figure 6 illustrates that Δoxy-Hb and Δdeoxy-Hb were rather heterogeneous between the rostral and caudal window sites in individual recordings. The caudal optode shows an increase of deoxy-Hb and a decrease of oxy-Hb consistent with a decrease of Hb oxygenation before the occurrence of the first SD, whereas there is no change at the rostral optode. Because Δoxy-Hb and Δdeoxy-Hb depend on CBF, these observations are in line with the findings of Group 1.

The EEG during both ET-1–induced SD and normal SD showed a short-lasting depression of activity and complete recovery. This pattern is typical of SDs but can also be observed in cases of peri-infarct depolarizations in the ischemic penumbra (25). If a cluster of SDs occurred, complete recovery of EEG activity was often not achieved before the next SD started.

Discussion

In rats under halothane anesthesia, a cortical microarea of selective neuronal necrosis was found whenever ET-1 (1 μ*M*) elicited SD, but not when ET-1 failed to trigger SD. Furthermore, a similar area of necrosis to that seen after ET-1–induced SD was also found when SD did not originate in

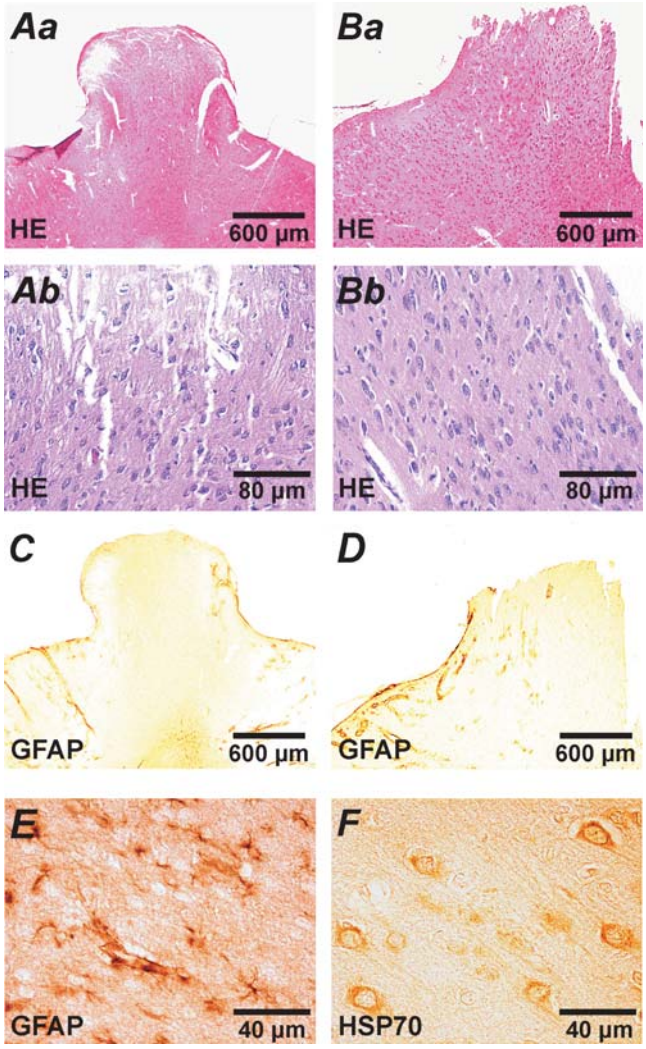

Figure 4. Histologic changes in cortex exposed to the combination of ET-1 with the ET_A receptor antagonist BQ-123, 24 hrs post-treatment. (Aa) Moderate edema but no areas of neuronal death were detected at Window 1 (high $[K^+]_{ACSF}$) using hematoxylin and eosin staining. (Ab) Larger magnification of (Aa). (Ba) Microareas of selective neuronal death were also completely absent from the area of Window 2 (ET-1 + BQ-123) in hematoxylin and eosin–stained sections. (Bb) Larger magnification of (Ba). (C) GFAP immunoreactivity was moderately increased in the cortex surrounding Window 1. (D) The same degree of GFAP immunoreactivity was detected in the cortex surrounding Window 2. (E) Larger magnification of (C). (F) Some neurons in the window area (in this case Window 1) demonstrated mild HSP70 immunoreactivity.

the ET-1–exposed cortex but invaded into this area from outside. If no SD propagated through the ET-1–exposed cortex, no neuronal damage occurred. These findings provide further evidence that SD causes neuronal damage under pathologic conditions (20, 26, 27). If SD propagated through the cortex under physiological conditions or was exposed to the combination of ET-1 and BQ-123, SD did not induce neuronal damage. This suggests that the damage induced by SD in the presence of ET-1 is related to ET_A receptor activation.

In models of cerebral ischemia, spreading depolarizations related to SD spontaneously occur in the ischemic penumbra (25–27). This is probably related to the gradual increase of the baseline extracellular K^+ concentration during energy compromise (28, 29), which appears to reflect activation of a Ca^{2+}- or ATP-gated K^+ current in conjunction with a decline in Na, K-ATPase activity (30). In contrast to SDs under normal conditions, penumbral spreading depolarizations seem to induce neuronal damage. Thus, the number of spreading depolarizations correlates with the infarct size (31, 32); there is a temporal correlation between occurrence of spreading depolarizations and the dynamics of infarct growth (33); and spreading depolarizations that are artificially triggered outside of the penumbra and propagate into it cause enlargement of the ischemic core (26, 27). We here show that SDs in the presence of ET-1 share this behavior with penumbral spreading depolarizations, and this provides an argument that ET-1 produces a penumbra-like condition *via* its vasoconstrictive action. In an earlier paper, it was already shown that the receptor profile is consistent with this hypothesis, as ET_A receptors only mediated ET-1–induced SD (18). Furthermore, it was demonstrated using K^+-sensitive microelectrodes that changes of the extracellular K^+ concentration typical of ischemia preceded the first ET-1–induced SD (13), and ET-1 failed to elicit SD in brain slices that are devoid of a blood circulation (13).

However, the measurements of CBF with laser-Doppler flowmetry did not give clear evidence that ET-1 produced an ischemic penumbra-like condition. Spectroscopic recordings of oxy-Hb and deoxy-Hb may be more sensitive than laser-Doppler flowmetry for detection of an ischemic region, because hemoglobin oxygenation depends not only on CBF but also on tissue oxygen consumption, which is increased by SD (34). However, similarly to the measurements of CBF, the recordings of cortical Δoxy-HB and Δdeoxy-Hb failed to demonstrate clear fingerprints of an ischemic penumbra (23). All this may reflect methodologic problems of laser-Doppler flowmetry and spectroscopy, which share a relatively low spatial resolution. In principle, ET-1, in the concentration range used here, is a potent vasoconstrictor of cerebral arteries. Thus, when directly applied to the middle cerebral artery, a concentration of 1 µ*M* was sufficient to produce severe arterial spasm and ischemic damage in the vascular territory (35). On the other hand, when ET-1 was topically applied to the neocortex under halothane, a higher concentration of 40 µ*M* was necessary to produce a significant decrease in CBF and ischemic damage (36). The latter dose-response relationship is consistent with our findings, as 1 µ*M* topically applied under halothane did not cause a significant decrease of CBF before the first SD. However, laser Doppler flowmetry measures CBF in a relatively large tissue volume between 0.5 and 1 mm^3. Thus, a small area of local ischemia may escape detection. Interestingly, the CBF pattern was apparently heterogeneous between different recording sites in our study. In individual recordings, a decrease of CBF at one and an increase at the

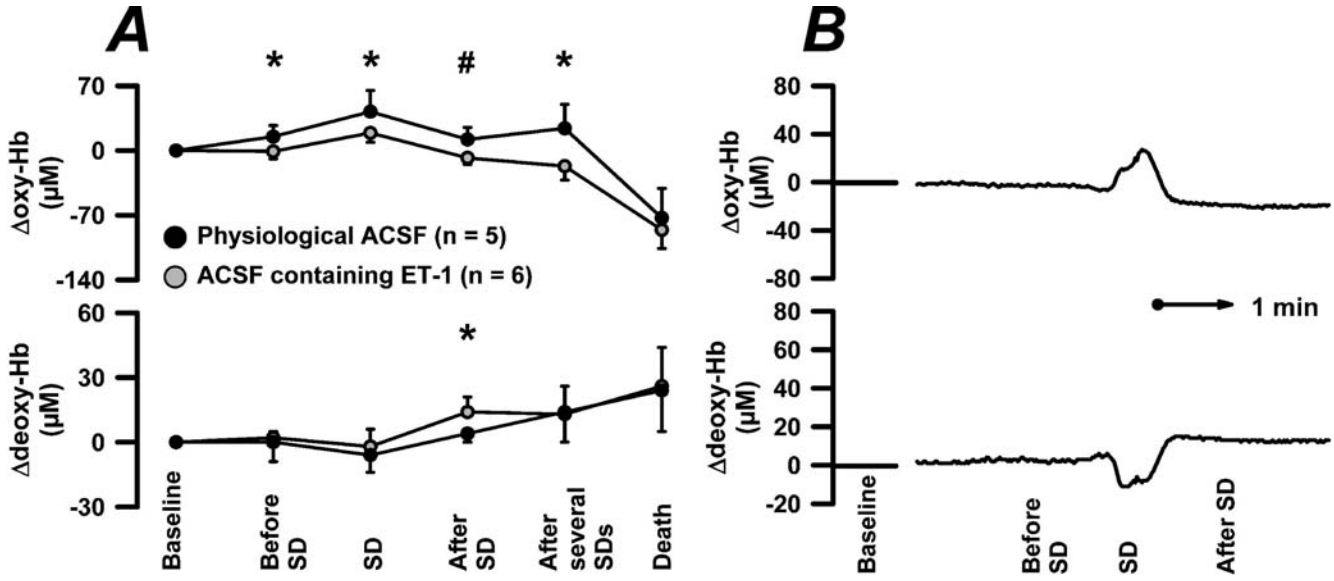

Figure 5. Changes in cortical oxy-Hb and deoxy-Hb concentrations associated with SD. (A) Comparison of changes in oxy-Hb and deoxy-Hb between the first SD in the presence of ET-1 ($n = 6$) and the first remotely-induced SD propagating through a cranial window superfused with physiological ACSF ($n = 5$). Δoxy-Hb was mildly but significantly lowered by ET-1 during all phases of SD, but the difference was relatively small. $^*P < 0.05$; $\#P < 0.01$. (B) Representative recording to illustrate when the changes in oxy-Hb and deoxy-Hb were measured in relation to SD.

other recording site was frequently observed. This behavior was not seen in controls. A similar heterogeneity was also observed using spectroscopy. The cause of the assumed local heterogeneity of CBF is unclear, but it could be a function of diffusion of ET-1 into the tissue or the collateralization in the cortex, as well as a diverse reactivity of different arteriolar segments to ET-1. In summary, it is possible that a very small area of ischemia surrounded by reactive hyperemia was hidden behind the heterogeneity of the CBF changes between the different recording sites. The finding of a microarea of selective neuronal necrosis at any rate is consistent with this hypothesis.

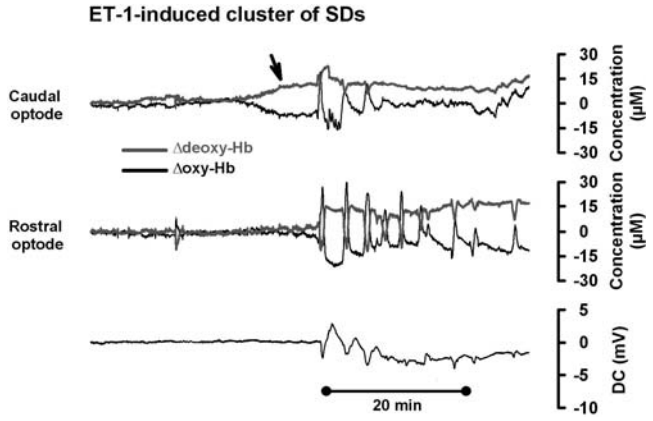

Figure 6. Representative changes in oxy-Hb and deoxy-Hb concentration associated with a cluster of SDs elicited by superfusion of the cortical surface with 1 μ*M* ET-1. ΔOxy-Hb and Δdeoxy-Hb were measured by spectroscopy, and SD was recorded as changes in the DC potential. There was a pronounced drop of oxy-Hb and rise of deoxy-Hb at the caudal optode before the first ET-1–induced SD (arrow), whereas no change is observed rostrally. The changes of oxy-Hb and deoxy-Hb depend on CBF. These findings appear to confirm the heterogeneity of CBF in response to ET-1 (1 μ*M*) as measured with laser Doppler flowmetry.

The ET-1 model of SD may be seen from a broader perspective as an example in which an ischemic microarea gives rise to the pathophysiological correlate of the migraine aura. In this way, a dysfunction in an area too small to be of functional significance could be perceived by a patient as it gives rise to SD and thereby a neuronal disturbance is carried to a by far larger volume of tissue. Very likely, the cause of microischemia does not necessarily have to be vasoconstriction, but could also be a small embolus. This could provide a straightforward explanation for another clinically well-established association, namely that between migraine aura and patent foramen ovale (37). In fact, there may be two major groups of migraine aura variants, one in which the trigger for SD is primarily neuronal or astroglial, such as in familial hemiplegic migraine, and another group in which the trigger is vascular. Based on our histologic findings, the latter in particular could have some significance as substrate of a progressive brain disorder (38–40).

ET-1–induced SD was inhibited by halothane, as are K^+-induced SDs (41). The mechanism underlying this effect is unclear. It has been speculated to be because of halothane's ability to inhibit gap junctions (42). However, ET-1 by itself is a potent gap junction inhibitor (43), which makes it somewhat unlikely that gap junction inhibition can markedly inhibit ET-1–induced SD. The inhibition of ET-1–induced SD by halothane could also be related to more directly antagonistic effects of halothane versus ET-1. Thus, vasoconstriction by ET-1 in rat aortic rings as well as ET-1–induced astroglial Ca^{2+} increases unrelated to gap junction permeability were found to be inhibited by halothane *in*

vitro (44, 45). Furthermore, if vasoconstriction is the cause of ET-1–induced SD, the inhibitory effect of halothane could also be related to its capability to increase CBF (46).

1. Wolff HG. Headache and Other Head Pain (6th ed.). New York: Oxford University Press, 1963.
2. Leão AAP, Morison RS. Propagation of spreading cortical depression. J Neurophysiol 8:33–45, 1945.
3. Nedergaard M, Hansen AJ. Spreading depression is not associated with neuronal injury in the normal brain. Brain Res 449:395–398, 1988.
4. Lauritzen M. Pathophysiology of the migraine aura. The spreading depression theory. Brain 117:199–210, 1994.
5. Hadjikhani N, Sanchez Del Rio M, Wu O, Schwartz D, Bakker D, Fischl B, Kwong KK, Cutrer FM, Rosen BR, Tootell RB, Sorensen AG, Moskowitz MA. Mechanisms of migraine aura revealed by functional MRI in human visual cortex. Proc Natl Acad Sci U S A 98: 4687–4692, 2001.
6. Janzen R, Tanzer A, Zschocke S, Dieckmann H. Postangiographische Spätreaktionen der Hirngefäße bei Migränekranken. Z Neurol 201:24–42, 1972.
7. Lassen NA, Friberg L. Cerebral blood flow measured by xenon 133 using the intraarterial injection method or inhalation combined with SPECT in migraine research. In: Olesen J, Ed. Migraine and Other Headaches. The Vascular Mechanisms. New York: Raven Press, pp5–13, 1991.
8. Olesen J, Friberg L, Olsen TS, Andersen AR, Lassen NA, Hansen PE, Karle A. Ischaemia-induced (symptomatic) migraine attacks may be more frequent than migraine-induced ischaemic insults. Brain 116:187–202, 1993.
9. Dichgans M, Mayer M, Uttner I, Bruning R, Muller-Hocker J, Rungger G, Ebke M, Klockgether T, Gasser T. The phenotypic spectrum of CADASIL: clinical findings in 102 cases. Ann Neurol 44:731–739, 1988.
10. Call GK, Fleming MC, Sealfon S, Levine H, Kistler JP, Fisher CM. Reversible cerebral segmental vasoconstriction. Stroke 19:1159–1170, 1988.
11. Bousser MG, Welch KM. Relation between migraine and stroke. Lancet Neurol 4:533–542, 2005.
12. Yanagisawa M, Kurihara H, Kimura S, Tomobe Y, Kobayashi M, Mitsui Y, Yazaki Y, Goto K, Masaki T. A novel potent vasoconstrictor peptide produced by vascular endothelial cells. Nature 332:411–415, 1988.
13. Dreier JP, Kleeberg J, Petzold G, Priller J, Windmuller O, Orzechowski HD, Lindauer U, Heinemann U, Einhaupl KM, Dirnagl U. Endothelin-1 potently induces Leao's cortical spreading depression in vivo in the rat: a model for an endothelial trigger of migrainous aura? Brain 125: 102–112, 2002.
14. Gallai V, Sarchielli P, Firenze C, Trequattrini A, Paciaroni M, Usai F, Palumbo R. Endothelin 1 in migraine and tension-type headache. Acta Neurol Scand 89:47–55, 1994.
15. Kallela M, Färkkilä M, Saijonmaa O, Fyhrquist F. Endothelin in migraine patients. Cephalgia 18:329–332, 1998.
16. Hasselblatt M, Kohler J, Volles E, Ehrenreich H. Simultaneous monitoring of endothelin-1 and vasopressin plasma levels in migraine. Neuroreport 10:423–425, 1999.
17. Tzourio C, El Amrani M, Poirier O, Nicaud V, Bousser MG, Alperovitch A. Association between migraine and endothelin type A receptor (ETA –231 A/G) gene polymorphism. Neurology 56:1273–1277, 2001.
18. Kleeberg J, Petzold GC, Major S, Dirnagl U, Dreier JP. ET-1 induces cortical spreading depression *via* activation of the ETA receptor/phospholipase C pathway in vivo. Am J Physiol Heart Circ Physiol 286: H1339–H1346, 2004.
19. Kohl M, Lindauer U, Royl G, Kuhl M, Gold L, Villringer A, Dirnagl U. Physical model for the spectroscopic analysis of cortical intrinsic optical signals. Phys Med Biol 45:3749–3764, 2000.
20. Dreier JP, Ebert N, Priller J, Megow D, Lindauer U, Klee R, Reuter U, Imai Y, Einhaupl KM, Victorov I, Dirnagl U. Products of hemolysis in the subarachnoid space inducing spreading ischemia in the cortex and focal necrosis in rats: a model for delayed ischemic neurological deficits after subarachnoid hemorrhage? J Neurosurg 93:658–666, 2000.
21. Herrera DG, Maysinger D, Almazan G, Funnel R, Cuello AC. Analysis of c-Fos and glial fibrillary acidic protein (GFAP) expression following topical application of potassium chloride (KCl) to the brain surface. Brain Res 784:771–781, 1998.
22. Dreier JP, Korner K, Ebert N, Gorner A, Rubin I, Back T, Lindauer U, Wolf T, Villringer A, Einhaupl KM, Lauritzen M, Dirnagl U. Nitric oxide scavenging by hemoglobin or nitric oxide synthase inhibition by N-nitro-L-arginine induces cortical spreading ischemia when K^+ is increased in the subarachnoid space. J Cereb Blood Flow Metab 18: 978–990, 1998.
23. Wolf T, Lindauer U, Reuter U, Back T, Villringer A, Einhaupl K, Dirnagl U. Noninvasive near infrared spectroscopy monitoring of regional cerebral blood oxygenation changes during peri-infarct depolarizations in focal cerebral ischemia in the rat. J Cereb Blood Flow Metab 17:950–954, 1997.
24. Kohl M, Lindauer U, Dirnagl U, Villringer A. Separation of changes in light scattering and chromophore concentrations during cortical spreading depression in rats. Opt Lett 23:555–557, 1998.
25. Nallet H, MacKenzie ET, Roussel S. The nature of penumbral depolarizations following focal cerebral ischemia in the rat. Brain Res 842:148–158, 1999.
26. Busch E, Gyngell ML, Eis M, Hoehn-Berlage M, Hossmann KA. Potassium-induced cortical spreading depressions during focal cerebral ischemia in rats: contribution to lesion growth assessed by diffusion-weighted NMR and biochemical imaging. J Cereb Blood Flow Metab 16:1090–1099, 1996.
27. Takano K, Latour LL, Formato JE, Carano RA, Helmer KG, Hasegawa Y, Sotak CH, Fisher M. The role of spreading depression in focal ischemia evaluated by diffusion mapping. Ann Neurol 39:308–318, 1996.
28. Nedergaard M, Hansen AJ. Characterization of cortical depolarizations evoked in focal cerebral ischemia. J Cereb Blood Flow Metab 13:568–574, 1993.
29. Muller M, Somjen GG. Na(+) and K(+) concentrations, extra- and intracellular voltages, and the effect of TTX in hypoxic rat hippocampal slices. J Neurophysiol 83:735–745, 2000.
30. Nowicky AV, Duchen MR. Changes in [Ca2+]i and membrane currents during impaired mitochondrial metabolism in dissociated rat hippocampal neurons. J Physiol 507:131–145, 1998.
31. Gill R, Andine P, Hillered L, Persson L, Hagberg H. The effect of MK-801 on cortical spreading depression in the penumbral zone following focal ischaemia in the rat. J Cereb Blood Flow Metab 12:371–379, 1992.
32. Mies G, Iijima T, Hossmann KA. Correlation between peri-infarct DC shifts and ischaemic neuronal damage in rat. Neuroreport 4:709–711, 1993.
33. Hartings JA, Rolli ML, Lu XC, Tortella FC. Delayed secondary phase of peri-infarct depolarizations after focal cerebral ischemia: relation to infarct growth and neuroprotection. J Neurosci 23:11602–11610, 2003.
34. Selman WR, Lust WD, Pundik S, Zhou Y, Ratcheson RA. Compromised metabolic recovery following spontaneous spreading depression in the penumbra. Brain Res 999:167–174, 2004.
35. Macrae M, Robinson MJ, Graham DI, Reid JL, McCulloch J. Endothelin-1-induced reductions in cerebral blood flow: dose dependency, time course, and neuropathological consequences. J Cereb Blood Flow Metab 13:276–284, 1993.

36. Fuxe K, Bjelke B, Andbjer B, Grahn H, Rimondini R, Agnati LF. Endothelin-1 induced lesions of the frontoparietal cortex of the rat. A possible model of focal cortical ischaemia. Neuroreport 8:2623–2629, 1997.
37. Wilmshurst PT, Nightingale S, Walsh KP, Morrison WL. Effect on migraine of closure of cardiac right-to-left shunts to prevent recurrence of decompression illness or stroke or for haemodynamic reasons. Lancet 356:1648–1651, 2000.
38. Kruit MC, van Buchem MA, Hofman PA, Bakkers JT, Terwindt GM, Ferrari MD, Launer LJ. Migraine as a risk factor for subclinical brain lesions. JAMA 291:427–434, 2004.
39. Kruit MC, Launer LJ, van Buchem MA, Terwindt GM, Ferrari MD. MRI findings in migraine. Rev Neurol (Paris). 161:661–665, 2005.
40. Goadsby PJ. Is migraine a progressive disorder? Considering the clinical implications of new research data on migraine and brain lesions. Med J Aust 182:103–104, 2005.
41. Saito R, Graf R, Hubel K, Taguchi J, Rosner G, Fujita T, Heiss WD. Halothane, but not alpha-chloralose, blocks potassium-evoked cortical spreading depression in cats. Brain Res 699:109–115, 1995.
42. Nedergaard M, Cooper AJ, Goldman SA. Gap junctions are required for the propagation of spreading depression. J Neurobiol 28:433–444, 1995.
43. Blomstrand F, Venance L, Siren AL, Ezan P, Hanse E, Glowinski J, Ehrenreich H, Giaume C. Endothelins regulate astrocyte gap junctions in rat hippocampal slices. Eur J Neurosci 19:1005–1015, 2004.
44. Boillot A, Vallet B, Marty J, Auclerc A, Barale F. Effects of halothane, enflurane and isoflurane on contraction of rat aorta induced by endothelin-1. Br J Anaesth 75:761–767, 1995.
45. Venance L, Premont J, Glowinski J, Giaume C. Gap junctional communication and pharmacological heterogeneity in astrocytes cultured from the rat striatum. J Physiol 1510:429–440, 1998.
46. Linde R, Schmalbruch IK, Paulson OB, Madsen PL. The Kety-Schmidt technique for repeated measurements of global cerebral blood flow and metabolism in the conscious rat. Acta Physiol Scand 165:395–401, 1999.